PROCEEDINGS OF SCIENCE

Indirect Techniques in Nuclear Astrophysics: Asymptotic Normalization Coefficients and the Trojan Horse Method

R.E. Tribble*
Cyclotron Institute, Texas A&M University
College Station, Texas, USA
E-mail: tribble@comp.,tamu.edu

T. Abdullah, C. Fu, C. Gagliardi, A. Mukhamedzhanov, G. Tabacaru, X. Tang, L. Trache
Cyclotron Institute, Texas A&M University
College Station, Texas, USA

P. Bem, V. Burjan, V. Kroha, J. Piskor, E. Simeckova, J. Vincour
Institute for Nuclear Physics , Czech Academy of Sciences
Prague-Rez, Czech Republic

F. Carstoiu
Institute for Atomic Physics
Bucharest, Romania

S. Spitaleri, S. Cherubini, V. Crucilla, M. La Cognata, L. Lamia, R.G. Pizzone, S. Romano, A. Tumino
Universita di Catania and INFN-Laboratori Nazionali del Sud
Catania, Italy

Both direct and indirect techniques have been used for many years to determine nuclear reaction rates at astrophysical energies. A number of problems have been encountered which limit measurements by direct techniques, including very low cross sections, the importance of subthreshold states and the need for radioactive targets. Over the past decade, new indirect techniques have been developed to help overcome some of these problems. In this contribution, two new techniques—Asymptotic Normalization Coefficients and the Trojan Horse Method—are described. Examples of their use in defining astrophysical reaction rates are also presented.

International Symposium on Nuclear Astrophysics – Nuclei in the Cosmos – IX
CERN, Geneva, Switzerland
25-30 June, 2006

* Speaker

PoS(NIC-IX)022

1. Introduction

Understanding stellar evolution requires detailed information about nuclear reactions and decays which are important in nuclear burning processes that provide energy to a star. The burning process is complicated, involving sequences of capture reactions and beta decays, and depends on density, temperature and nuclear abundances. Reaction and decay cycles, beginning with the *p-p* chain and extending to the *CNO*, *Ne-Na*, etc., cycles, process the nuclear fuel, primarily through hydrogen and helium burning, yielding increasingly massive nuclei and producing energy. Explosive stellar processes involve similar sequences of reactions and decays. Some of the important reactions in the burning cycles and most in explosive processes involve unstable nuclei. Direct and indirect techniques utilizing radioactive beams are now being used to measure these reaction rates.

2. Indirect Techniques

A number of indirect techniques have been used to determine reaction rates at stellar energies. For many years, measurements of resonance energies and radiative and charged-particle widths have been carried out to predict resonant capture reaction rates. Starting in the early '90's, these measurements have been extended to radioactive 'targets.' Also in the '90's new indirect techniques were developed. One of these, Coulomb dissociation, is the subject of another contribution to these proceedings. Two others—asymptotic normalization coefficients (ANCs) and the Trojan Horse method (THM)—are described here.

The ANC technique is based on the fact that direct proton-capture reactions of astrophysical interest involve systems where the binding energy of a captured charged particle is low. Hence at stellar energies, the capture proceeds through the tail of the nuclear overlap function. The shape of the overlap function in this tail region is completely determined by the Coulomb interaction, so the amplitude of the overlap function alone dictates the rate of the capture reaction. The asymptotic normalization coefficient (ANC), C, for the system $A + p \leftrightarrow B$ specifies the amplitude of the tail of the overlap function. Astrophysical S factors for peripheral direct radiative capture reactions can be determined through measurements of ANC's using traditional nuclear reactions such as peripheral nucleon transfer, elastic scattering and breakup reactions. The ANC is connected to both the resonant and nonresonant capture amplitudes, and it can be used to determine astrophysical S factors when the capture occurs through a subthreshold resonance state [1].

The THM has been used to study charged particle transfer reactions down to very low separation energies. The technique utilizes a projectile which includes the particle to be transferred and a spectator. The ground state of the projectile should have a strong overlap with a cluster configuration for the two components. The projectile penetrates the Coulomb barrier of the target and the particle of interest is transferred while the spectator flies off. If quasi-free kinematics are chosen, the reaction emulates the transfer of a charged particle on a bare nucleus. Thus by using the THM, charged particle transfer reactions can be studied at very low projectile energies without interference from electron screening effects.

3. The ANC Technique

It is well known that capture of a charged particle at stellar energies occurs at distances that are large compared to the nuclear radius. Direct capture-gamma reaction rates depend on the normalization of the overlap function which is fixed by the appropriate ANCs. The connection between ANCs and direct proton capture rates at low energies is straightforward to obtain. The cross section for the direct capture reaction *A(p,γ)B* can be written as

$$\sigma = \lambda \left| < I_{Ap}^{B}(\boldsymbol{r}) \middle| \hat{O}(\boldsymbol{r}) \middle| \psi_i^{(+)}(\boldsymbol{r}) > \right|^2, \quad (1)$$

where λ contains kinematical factors, $I_{Ap}^{B}(\boldsymbol{r})$ is the overlap function for $B \to A + p$, $\hat{O}$ is the electromagnetic transition operator and $\psi_i^{(+)}$ is the scattering wave in the incident channel. If the dominant contribution to the matrix element comes from outside the nuclear radius, the overlap function may be replaced by

$$I_{Ap}^{B} \approx C \frac{W_{-\eta, l+1/2}(2\kappa r)}{r} \quad (2)$$

where *C*, the ANC, defines the tail of the radial overlap function, *W* is the Whittaker function, η and *l* are the Coulomb parameter and orbital angular momentum for the bound state *B* = *A* + *p* and κ is the bound state wave number. Thus direct capture cross sections are directly proportional to the squares of the ANCs. In a similar way, ANCs can be used to determine reaction rates for subthreshold states [1]. In addition, ANCs can be related to the external or channel part of the resonance width for resonant capture [1]. The internal part of the width, however, depends on the strength of the overlap function in the nuclear interior. If resonance parameters are known either from measurements or calculations and ANCs are known, the resonant and nonresonant components can be used together in an *R*-matrix calculation to obtain capture cross sections.

Peripheral transfer reactions provide an excellent way to determine ANCs. Consider the proton transfer reaction *A(a,c)B* where *a* = *c* + *p* and *B* = *A* + *p*. As was previously shown [2] we can write the DWBA cross section in the form

$$\frac{d\sigma}{d\Omega} = \sum_{j_B j_a} \frac{(C^{B}_{Apl_B j_B})^2 (C^{a}_{cpl_a j_a})^2}{b^2_{Apl_B j_B} b^2_{cpl_a j_a}} \tilde{\sigma}^{DW}_{l_B j_B l_a j_a}, \quad (3)$$

where $\tilde{\sigma}^{DW}_{l_B j_B l_a j_a}$ is the reduced DWBA cross section and j_i, l_i are the total and orbital angular momenta of the transferred proton in nucleus *i*. The factors $b_{cpl_a j_a}$ and $b_{apl_B j_B}$ are the ANCs of the bound state proton wave functions in nuclei *a* and *B* which are related to the corresponding ANC of the overlap function by

$$(C^{a}_{cpl_a j_a})^2 = S^{a}_{cpl_a j_a} b^2_{cpl_a j_a} \quad (4)$$

where $S^{a}_{cpl_a j_a}$ is the spectroscopic factor. If the reaction is peripheral, the ratio

$$R_{l_B j_B l_a j_a} = \frac{\tilde{\sigma}^{DW}_{l_B j_B l_a j_a}}{b^2_{Apl_B j_B} b^2_{cpl_a j_a}} \quad (5)$$

is independent of the single particle ANCs $b_{cpl_a j_a}$ and $b_{apl_B j_B}$. Thus for surface reactions where Eq. 5 holds, the DWBA cross section is best parametrized in terms of the product of the square of the ANCs of the initial and final nuclei $(C^B)^2(C^a)^2$. The ANC, C^B, is the same one that is needed in Eq. 2 to determine the capture reaction cross section defined in Eq. 1.

The ANC technique has been tested by comparing the *S* factor for the ground and first excited state of $^{16}O(p,\gamma)^{17}F$, which are pure direct capture reactions at low energies, with the predictions for the two states based on ANCs determined from the $^{16}O(^3He,d)^{17}F$ reaction. The two S factors agreed to better than 10% [3].

3.1 Applications of the ANC Technique

Many measurements of ANCs have been carried out in the past decade with both stable and radioactive beams. Below we give only a couple of examples of applications of the technique.

ANCs for $^{15}O \leftrightarrow {}^{14}N + p$ were measured using the $^{14}N(^3He,d)^{15}O$ reaction. The experiment was carried out with ^3He beams supplied by the U-120M isochronous cyclotron of the Nuclear Physics Institute near Prague, Czech Republic. A 26.3 MeV beam was used with a 260 μg/cm^2 melamine target ($C_3H_6N_6$) to measure the $^{14}N(^3He,d)^{15}O$ reaction. Reaction products were observed in a ΔE-E Si detector telescope. ANCs were obtained for the ground and five excited states in ^{15}O. The state that dominates the reaction rate at stellar energies through an *s*-wave capture is a subthreshold state at E_x = 6.79 MeV. Angular distributions for the states, including the important subthreshold state, along with DWBA predictions are given in [4].

The $^{14}N(p,\gamma)^{15}O$ reaction is one of the more important ones in the *CNO* cycle. As the slowest reaction in the cycle, it defines the rate of energy production and, hence, the lifetime of stars that are governed by hydrogen burning via *CNO* processing. The rate of this reaction has a major impact on the evolution of a wide range of stars. In 1987 the $^{14}N(p,\gamma)^{15}O$ reaction was remeasured and results were obtained for transitions to the ground and excited states of ^{15}O. From the measurements, the total astrophysical factor, $S(0)$ = 3.20 ± 0.54 keVb [5], was deduced. The measurement led to a new understanding of the capture reaction, however, since it was found that $^{14}N(p,\gamma)^{15}O$ capture at low energies is dominated by resonant and direct capture to the first resonance at E_{R1}=259.5 keV (the resonance energy in the c. m.) and a subthreshold resonance at E_s=-504 keV. At very low energies appropriate for stellar burning the reaction was found to be dominated by a combination of direct and resonant capture and interference through the tail of the subthreshold and the first resonance.

In 2001 the first measurement of the width of the subthreshold state was reported in [6]. The result was substantially smaller than had been used in the analysis reported in a direct measurement which led to $S(0)$ = 3.20 ± 0.54 keVb [5]. The small width indicated that direct capture through the subtrheshold state dominates the *S* factor at stellar energies. The ANC obtained by us was used to determine the *S* factor. The results are shown in Fig. 1. Our value for the S factor is S(0) = 1.62 ± 0.25 keVb [4] which is about a factor of two below the previously accepted value. After our results were published, new direct measurements were completed that

agreed with our result for the *S* factor [7]. The new results indicate that the energy production in the CNO cycle is smaller than previously estimated, which leads to a new lower limit on the age of the globular clusters, changing the old value by about 1 Gyr.

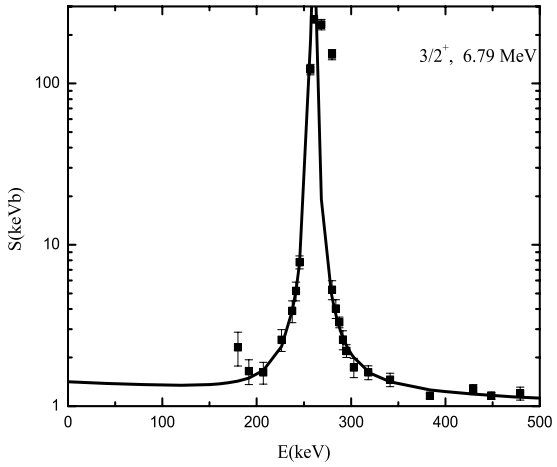

Figure 1. The result from an R-matrix fit for the *S* factor due to the subthreshold state in $^{14}N(p,\gamma)^{15}O$.

Recently a similar study has been carried out for $^{20}Ne(p,\gamma)^{21}Na$. In this case, the reaction rate is dominated by a subthreshold state which is bound by only a few keV. Unfortunately the gamma width of the subtrheshold resonance has not been measured which leads to a large uncertainty on the rate [8].

Using a secondary radioactive beam, we have measured the $^{14}N(^{13}N,^{14}O)^{13}C$ reaction to determine the ANCs for $^{14}O \leftrightarrow {}^{13}N + p$ and, in turn, the direct capture rate for $^{13}N(p,\gamma)^{14}O$ at astrophysical energies. For $T_9 = 0.2$, the Gamow window for the $^{13}N(p,\gamma)^{14}O$ reaction is located at 148 keV with a width of 117 keV. At this energy the reaction is dominated by the low-energy tail of the *s*-wave capture on the broad 1^- resonance at E_r=0.529 MeV. The direct capture contribution is significantly smaller than that due to the tail of the resonance within the Gamow window. But since both resonant and nonresonant capture proceed via *s* waves and then decay by *E1* transitions, there is an interference between the two components. Thus the resonant tail can be enhanced through constructive interference or reduced through destructive interference. We have used the ANC and the measured experimental resonance parameters [9] in an R-matrix calculation to obtain the *S* factor. The *S* factor from the calculation is shown together with the result from Decrock *et al.* [9], in Fig. 2. The relatively flat lower solid line, which is our result for direct capture alone, is about 30% larger than the result obtained by Decrock *et al.*, which is shown as the lowest dash-dotted line in the figure. The two results just agree within the quoted uncertainties. At $E_{c.m.}$ = 140 keV where the Gamow peak is located for $T_9 = 0.2$, our updated result using constructive interference, shown as the upper solid line, is about 38% higher than the previous result, which is shown as the upper dash-dotted line. This is due to the larger direct capture contribution from the ANC measurement. For completeness, we also show the result that would be obtained with destructive interference as the dashed line. With the *S* factor, the reaction rate has been calculated and is discussed in [10].

4. The Trojan Horse Method

The THM has proven to be very successful for studying charged particle two-body reactions relevant for astrophysics [11-14]. The THM replaces the $A + x \rightarrow c + C$ two-body

reaction by a suitable $A + a \rightarrow c + C + s$ three-body process, establishing a relation between the two reactions by using nuclear reaction theory. The nucleus, *a,* has a wave function with a large amplitude for an *x*-*s* cluster configuration. In a selected part of the three-body phase space where the other cluster *s* remains a spectator to the process, the three-body reaction can be regarded as an off-shell two-body reaction, usually referred to as a quasi-free reaction. Since the three-body process occurs at energies above the Coulomb barrier, the main feature is the suppression of both Coulomb barrier and screening effects in the off-shell two-body cross section. Nevertheless the quasi-free $A + x$ process can occur even at very low sub-Coulomb energies thanks to the key role of the *x*-*s* binding energy in compensating for the $A + a$ relative motion. This is a different approach to the THM compared to the original idea of Baur [15], where the initial velocity of the projectile *A* is compensated for by the Fermi motion of *x*. In that framework a quite large momentum, of the order of 200 MeV/c or more, is needed. But the relative yield of the experimental momentum distribution at such momenta can be very small, especially for $l = 0$ inter-cluster motion (for example *p*-*n* motion inside ^{2}H or α-*d* motion inside ^{6}Li). This would make the separation from other competitive reaction mechanisms very difficult. Moreover, the theoretical description of the tails of the momentum distribution can be complicated, their shape being very sensitive to it. In our approach to the THM, the inter-cluster motion is only needed to fix the accessible astrophysical energy region within a chosen cutoff in momentum, usually of the order of a few tens of MeV/c. In this framework, the so called "quasi-free two-body energy" is given by:

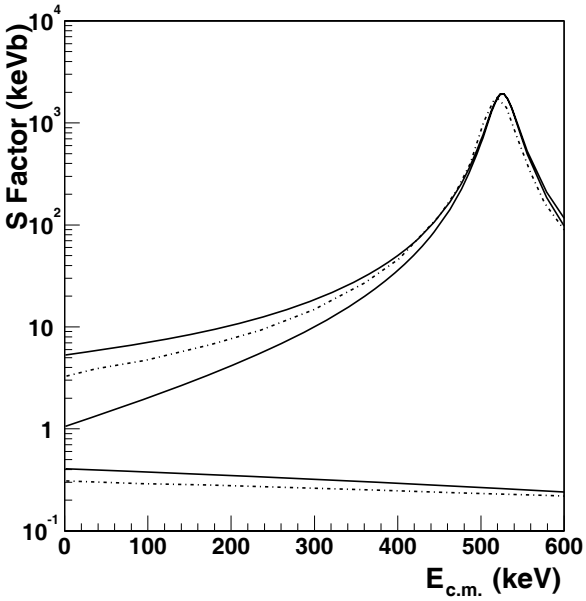

Figure 2. The result from an R-matrix fit for the *S* factor due to the ^{13}N(p,γ)^{14}O reaction. The nearly flat solid line gives our result for direct capture alone. The upper and lower solid lines give the total *S* factor with constructive and destructive interference, respectively. The dotted lines give the results found by Decrock *et al*. [9].

$$E_{q.f.} = E_{Ax} - B_{xs} \pm E_{xs} \quad (6)$$

where E_{Ax} is the beam energy in the center of mass of the $A + x$ two-body reaction, B_{xs} represents the binding energy of the two clusters *x* and *s*, and E_{xs} is related to the *x*-*s* intercluster motion.

Quasi-free processes have been exhaustively treated using the Plane Wave Impulse Approximation (PWIA), which provides a straightforward relation between three-body and two-body cross-sections. In particular, in PWIA the cross section of the A + a $\rightarrow$ c + C + s three body reaction can be factorized as given by

$$\frac{d^3\sigma}{dE_c d\Omega_c d\Omega_C} \propto KF \left(\frac{d\sigma}{d\Omega}\right)_{off} \mid \Phi(\boldsymbol{p}_{xs}) \mid^2 \quad (7)$$

where $\left(\frac{d\sigma}{d\Omega}\right)_{off}$ is the off-energy-shell differential cross section for the two body $A + x \rightarrow c + C$ reaction of interest at the center of mass energy E_{cm}, given in the post collision prescription by

$$E_{cm} = E_{cC} - Q_{2body} \quad (8)$$

where Q_{2body} is the two body Q-value of the $A + x \rightarrow c + C$ reaction and E_{cC} is the relative energy between the outgoing particles *c* and *C*; *KF* is a kinematical factor containing the final state phase-space factor. It is a function of the masses, momenta and angles of the outgoing particles and is given by

$$KF = \frac{\mu_{Aa} m_c}{(2\pi)^5 \hbar^7} \frac{k_C k_c^3}{k_{Aa}} \left[\left(\frac{\boldsymbol{k}_{Bx}}{\mu_{Bx}} - \frac{\boldsymbol{k}_{Cc}}{m_c} \right) \cdot \frac{\boldsymbol{k}_c}{k_c} \right]^{-1} \quad (9)$$

where *B* stands for the A + x → C + c system, $\boldsymbol{k}(\boldsymbol{p}_i)$ (m_i) is the momentum (mass) of the particle *i*, $\boldsymbol{k}_{ij}$ (μ_{ij}) is the relative momentum (reduced mass) of the real and virtual particle pairs *i* and *j*. The term $\Phi(\boldsymbol{p}_{xs})$ is the Fourier transform of the radial two cluster (xs) bound state wave function.

Eq. (7), which is used in the standard THM analysis, is based on the plane wave approximation in the initial channel of the TH reaction. If we take into account the Coulomb interaction between particles *A* and *a* in the entry channel, Eq. (7) should be replaced by the more accurate one:

$$\frac{d^3\sigma}{dE_c d\Omega_c d\Omega_C} \propto KF \left(\frac{d\sigma}{d\Omega}\right)_{off} |CR(\boldsymbol{k}_a, \boldsymbol{k}_s)|^2, \quad (10)$$

where

$$CR(\boldsymbol{k}_a, \boldsymbol{k}_s) = \int \frac{d\boldsymbol{p}_a}{(2\pi)^3} \psi^{(C)(+)}_{\boldsymbol{k}_a}(\boldsymbol{p}_a) \Phi(\boldsymbol{p}_{xs}) \quad (11)$$

is the Coulomb modified renormalization factor and $\psi^{(C)(+)}_{\mathbf{k}_a}(\mathbf{p}_a)$ is the Fourier transform of the Coulomb scattering wave function of particles *A* and *a* in the initial channel. Calculations show that the difference between the results obtained with the standard procedure and Coulomb modified renormalization factor does not exceed 7%.

Another important point to address is the absence of the Coulomb interaction in the initial channel of the cross section determined from the THM. The half-off-shell reaction amplitude of the direct sub-process $A + x \rightarrow C + c$ which is related with the differential cross section determined from the THM can be written as

$$M^{(off)}(\boldsymbol{k}_{Cc}, \boldsymbol{p}_{Ax}) = < \chi^{(-)}_{\boldsymbol{k}_{Cc}}(\boldsymbol{p}_{Cc}) \mid M^{(0)}(\boldsymbol{p}_{Cc}, \boldsymbol{p}_{Ax}) > . \quad (10)$$

Here, $M^{(0)}(\boldsymbol{k}_{Cc}, \boldsymbol{p}_{Ax})$ is the reaction amplitude in the plane wave approximation in the initial and final channels. To get the THM reaction amplitude $M^{(off)}(\boldsymbol{k}_{Cc}, \boldsymbol{p}_{Ax})$ we need to fold $M^{(0)}(\boldsymbol{k}_{Cc}, \boldsymbol{p}_{Ax})$ with the distorted wave $\chi^{(-)}_{\boldsymbol{k}_{Cc}}(\boldsymbol{p}_{Cc})$ describing the scattering of particles C and c in the final state while the initial state is described by the off-shell plane wave $|\boldsymbol{p}_{Ax}>$. In contrast the on-shell reaction amplitude (assuming that the reaction mechanism for the half-off-shell and on-shell processes is the same) is given by

$$M^{(on)}(\boldsymbol{k}_{Cc}, \boldsymbol{k}_{Ax}) = < \chi^{(-)}_{\boldsymbol{k}_{Cc}}(\boldsymbol{p}_{Cc}) | M^{(0)}(\boldsymbol{p}_{Cc}, \boldsymbol{p}_{Ax}) | \chi^{(+)}_{\boldsymbol{k}_{Ax}}(\boldsymbol{p}_{Ax}) >, \quad (11)$$

where $M^{(0)}(\boldsymbol{p}_{Cc}, \boldsymbol{p}_{Ax})$ is folded with the distorted waves in the initial and final channels. At low relative kinetic energy the initial state can be replaced by the pure Coulomb scattering wave function whose energy dependence is dominated by the Gamow factor. When calculating the astrophysical factor from the on-shell cross section, this Gamow factor is eliminated and the remaining energy behaviour, which is mainly determined by the hypergeometric function is very mild. The half-off-shell cross section determined from the THM does not contain the Gamow factor and gives directly the astrophysical factor whose energy behaviour is very close to the one obtained from the on-shell astrophysical factor.

Finally we address the importance of the off-shell effects on the energy behaviour of the astrophysical factor. In Fig. 3 we compare the on-shell and off-shell astrophysical factors calculated for two reactions, ^{7}Li(p,α)^{4}He and ^{6}Li(d,α)^{4}He. The calculations have been done assuming a triton transfer for the first reaction and deuteron transfer for the second. From Fig. 3, it is clear that the results which were calculated for quasi-free (QF) kinematics clearly justify the THM. The energy dependence of the half-off-shell and on-shell astrophysical factors are practically identical at low energies. Since only the energy dependence is of interest, the half-off-shell result in Fig. 3 has been normalized to the on-shell one at an energy E_{Ax} = 1 keV for ease of comparison.

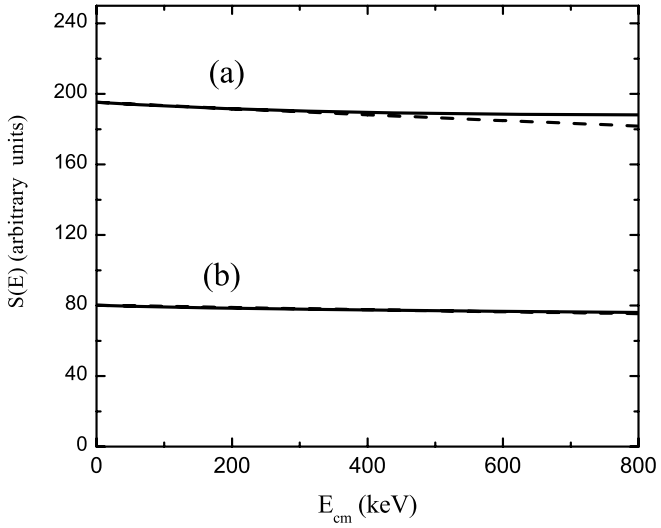

Figure 3. Energy dependence (E ≡ E_{Ax}) of the half-off-shell (dashed line) and on-shell (solid line) astrophysical factors for (a) the ^{7}Li(p,α)^{4}He reaction; (b) the ^{6}Li(d,α)^{4}He reaction.

4.1 Applications of the THM

The THM offers a unique way to measure the bare nucleus S(E) factor and has been applied to several astrophysically relevant reactions. Here we report only on a few of the many applications carried out so far.

The ^{3}He(d,p)α reaction was investigated via the THM by selecting the quasi-free (QF) contribution of the ^{6}Li(^{3}He,$p\alpha$)^{4}He three-body process off the α-particle from ^{6}Li [14]. This reaction is involved in the production of ^{2}H, ^{3}He, ^{4}He and ^{7}Li nuclear ashes from the early universe (homogeneous and inhomogeneous big bang nucleosynthesis), which are used to extract information on the baryon density of universe. Moreover the ^{3}He(d,p)α reaction is important for understanding the electron screening effect, since it shows a very pronounced enhancement in the cross-section at low energy, significantly larger than could be accounted for from the adiabatic limit. This effect prevents us from directly measuring the astrophysically relevant bare nucleus cross-section.

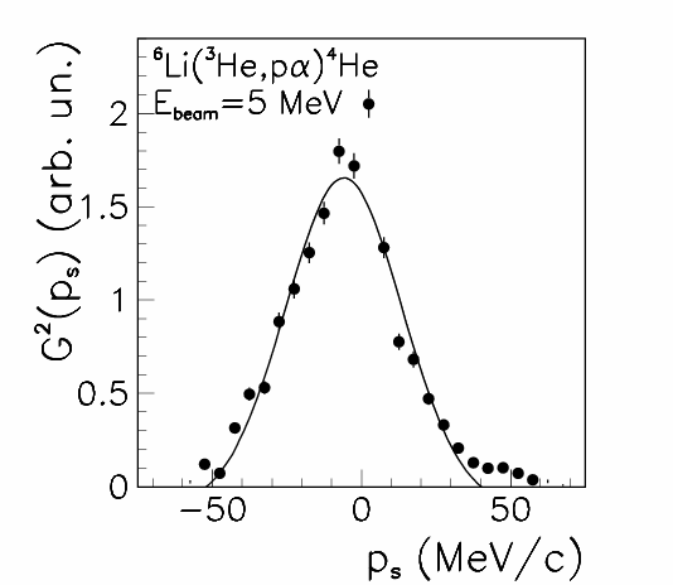

Figure 4. Experimental momentum distribution (full dots) compared with the theoretical one given in terms of a Hánkel function (solid line).

The ^{6}Li(^{3}He,$p\alpha$)^{4}He experiment was performed at the Dynamitron Tandem Laboratorium in Bochum (Germany). The 4 MV tandem accelerator provided a 5.6 MeV ^{3}He beam which was delivered onto an isotopically enriched lithium fluoride target (^{6}Li ~ 95%). The detection set-up consisted of two pairs of coincidence telescopes (annular silicon ΔE- plus silicon Position Sensitive E-Detectors) arranged symmetrically on opposite sides of the beam direction. The selected angular ranges, 9°-23° for α's and 136°-156° for protons, correspond to a momentum of the undetected α particle ranging from –100 to 100 MeV/c. This assures that the bulk of the quasi-free contributions of the breakup process fall within the experimental phase space region. As known, the analysis of the experimental results is in general complicated by the presence of other reaction mechanisms feeding the same particles in the three-body final state, e.g. sequential decay and direct break-up. In particular, a strong sequential decay from the first exited state of ^{8}Be ($J^{\pi} = 2^{+}$, E_x = 3.04 MeV and Γ = 1.5 MeV) appears to populate the α + α + p exit channel. This contribution was subtracted before extracting the S(E)-factor for the two-body reaction (see ref. [14] for details). Then a detailed study of the shape of the experimental momentum distribution for the spectator α was performed with the remaining events. A Hánkel like shape shows up (see Fig.4), with a FWHM of about 40 MeV/c, which agrees with the value from the literature for the α-d system inside ^{6}Li [16]. Following Eq.7, the two-body cross

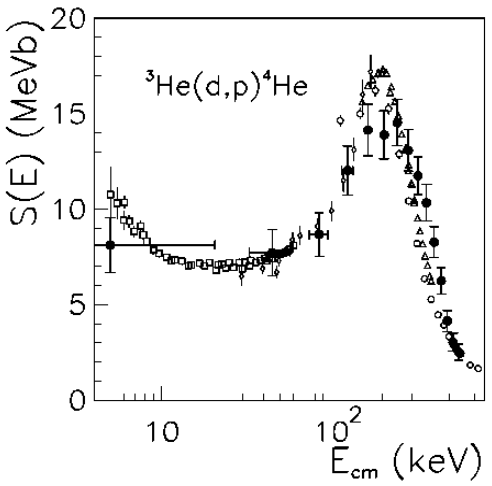

Figure 5. Astrophysical S(E) factor for the ^{3}He(d,p)^{4}He reaction (full dots) compared with direct data from [16] (open squares), [17] (open triangles), [18] (open diamonds), [19] (open circles).

section $\left(\frac{d\sigma}{d\Omega}\right)_{off}$, and then the S(E)-factor, was derived dividing the selected three-body experimental coincidence yield by the result of a Monte Carlo calculation based on the MPWBA [14]. The momentum distribution entering the calculation is a Hánkel function and the geometrical efficiency of the experimental set-up as well as the detection thresholds of the detectors were taken into account. The normalization to the direct excitation function [17-20] was performed in the region between 100 and 600 keV, corresponding to the resonance in the ^{4}He + p two-body channel, associated with the 16.66 MeV state of ^{5}Li. Figure 5 shows the extracted S(E) factor compared with the direct one, both averaged over the same bin energy of 40 keV. In spite of the low statistics both data sets show the same energy trend above E_{cm} = 20 keV and also the ^{5}Li resonance is well reproduced. Our estimates for the bare nucleus S(0) parameter and the U_e screening potential, S(0)=6.8 ± 1.4 MeV b and U_e = 155 ± 34 eV, are in agreement within experimental errors from previous results, but also confirm the adiabatic limit.

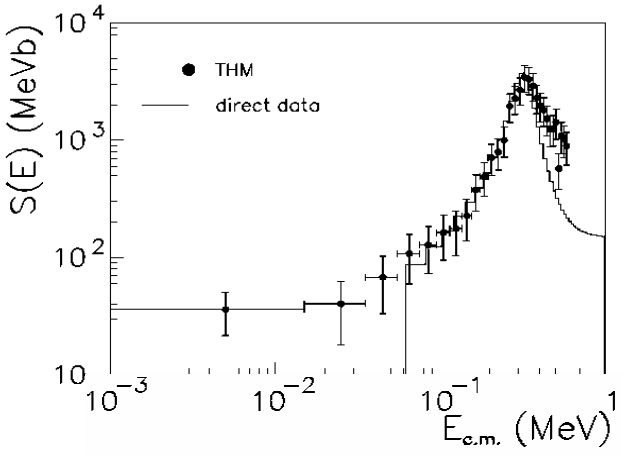

Figure 6. THM S(E) factor for the ^{15}N(p,α)^{12}C reaction (full dots) and direct data from [21,22,23] in the low energy region (solid line).

The THM was recently applied to the ^{2}H(^{15}N,α^{12}C)n process to measure the low-energy bare-nucleus cross section for the ^{15}N(p,α)^{12}C reaction [22]. The rate for this reaction, which is responsible for removing proton and ^{15}N nuclei from the ^{19}F production chain in the AGB intershell environment, is not well known. This introduces about a 10% uncertainty in the fluorine surface abundance, which is a strong constraint in AGB star modes. The experiment was performed at the Texas A&M University Cyclotron Institute. The K500 superconducting cyclotron provided

a 60 MeV ^{15}N beam which was delivered onto a self supporting CD_2 target of about 150 μg/cm^2 thickness. The detection setup consisted of a telescope (ionisation chamber for ΔE and a position sensitive detector (PSD) for $E_{residual}$) to discriminate carbon nuclei, and of two silicon PSDs placed on the opposite side of the beam direction. The angular ranges were chosen in such a way to cover the phase space region relevant for the QF mechanism. The analysis was carried out following the same procedure as above [21]. An error calculation for the E_{cm} variable was performed by means of standard formulas leading to a value ranging from 10 to 40 keV. Then, direct data from [22-24] were smeared out in order to be compared with THM data. Preliminary results are reported in Fig. 6. The full dots are THM data while direct data are reported as a solid line. The data sets agree reasonably well in the region of the resonance associated with the 12.44 MeV $J^{\pi} = 1^-$ state of ^{16}O. No direct data are available below 70 keV. In this region our data strongly disagree with R-matrix calculations/extrapolations from direct data performed to get the S(0) value. Our preliminary estimate from only one set of coincidence data is S(0) = 37 ± 11 MeV b, which is about a factor 2 lower than the direct result. A destructive interference between the 12.44 MeV level of ^{16}O with a sub-threshold state at 9.58 MeV of excitation energy (not considered in the calculations performed on the direct data) seems to be responsible for this behaviour. Work is in progress to understand this effect and its astrophysical implications.

5. Acknowledgements

At Texas A&M University, this work was supported in part by the U.S. Department of Energy under Grant No. DE-FG03-93ER40773, the U.S. National Science Foundation under Grant No. INT-9909787, ME 385(2000) project NSF and MSMT, CR, grant GACR 202/01/0709, and by the Robert A. Welch Foundation.

References

[1] A.M. Mukhamedzhanov and R.E. Tribble, Phys. Rev. C **59** (1999) 3418.

[2] A.M. Mukhamedzhanov, *et al*., Phys. Rev. C **56** (1997) 1302.

[3] C.A. Gagliardi *et al*., Phys. Rev. C **59** (1999) 1149.

[4] A.M. Mukhamedzhanov, *et al*., Phys. Rev. C **67** (2003) 065804.

[5] U. Schroeder *et al*., Nucl. Phys. A 467 (1987), 240.

[6] P.F. Bertone *et al*., Phys. Rev. Lett. 87 (2001) 152201.

[7] A. Formicola et al., Phys. Lett. B **591** (2004) 61.

[8] A.M. Mukhamedzhanov, *et al*., Phys. Rev. C **73** (2006) 035806.

[9] P. Decrock *et al.*, Phys. Rev. C **48** (1993) 2057.

[10] Xiadong Tang *et al*., Phys Rev. C **69** (2004) 055807.

[11] C. Spitaleri et al., Phys. Rev. C **63** (2001) 055801.

[12] A. Tumino et al., Phys. Rev. C **67** (2003) 065803.

[13] C. Spitaleri et al., Phys. Rev. C **69** (2004) 055806.

[14] M. La Cognata et al., Phys. Rev. C **72** (2005) 065802.

[15] G. Baur, Phys. Lett. B **178** (1986) 135.

[16] S. Barbarino et al., Phys. Rev. C **21** (1980) 1104.

[17] M.L. Aliotta et al., Nucl. Phys. A**690** (2001) 790.

[18] W.H. Geist et al., Phys. Rev. C **60** (2001) 054003.

[19] A.Krauss et al., Nucl. Phys. A **465** (1987) 150.

[20] T.W. Bonner et al., Phys. Rev. **88** (1952) 473.

[21] M. La Cognata et al., Eur. Phys. J. A (2005) DOI: 10.1140/epja/i2006-08-034-5.

[22] Redder et al., Z. Phys. A **305** (1982) 325.

[23] A. Schardt et al., Phys. Rev. **86** (1952) 527.

[24] J.L. Zyskind et al., Nucl. Phys. A **320** (1979) 404.